Title

Role of MnO2 in controlling iron and arsenic mobilization from illuminated flooded arsenic-enriched soils

Authors

Dong, Guowen
Han, Ruiwen
Pan, Yajing
et al.

Publication Date

2021

DOI

10.1016/j.jhazmat.2020.123362

Peer reviewed

Journal of Hazardous Materials 401 (2021) 123362

Contents lists available at ScienceDirect

Journal of Hazardous Materials

journal homepage: www.elsevier.com/locate/jhazmat

Role of MnO_2 in controlling iron and arsenic mobilization from illuminated flooded arsenic-enriched soils

Guowen Dong[a,b], Ruiwen Han[a], Yajing Pan[a], Chengkai Zhang[a], Yu Liu[a], Honghui Wang[d], Xiaoliang Ji[a], Randy A. Dahlgren[a,c], Xu Shang[a], Zheng Chen[a,d,e,*], Minghua Zhang[a,c]

[a] Zhejiang Provincial Key Laboratory of Watershed Science & Health, School of Public Health and Management, Wenzhou Medical University, Wenzhou, 325035, People's Republic of China
[b] Fujian Provincial Key Laboratory of Resource and Environment Monitoring & Sustainable Management and Utilization, College of Resources and Chemical Engineering, Sanming University, Sanming, 365000, People's Republic of China
[c] Department of Land, Air and Water Resources, University of California, Davis, Davis, CA, 95616, United States
[d] Department of Environmental Science, School of Environmental Science & Engineering, Tan Kah Kee College, Xiamen University, Zhangzhou, 363105, People's Republic of China
[e] Fujian Provincial Key Lab of Coastal Basin Environment, Fujian Polytechnic Normal University, Fuqing, 350300, People's Republic of China

GRAPHICAL ABSTRACT

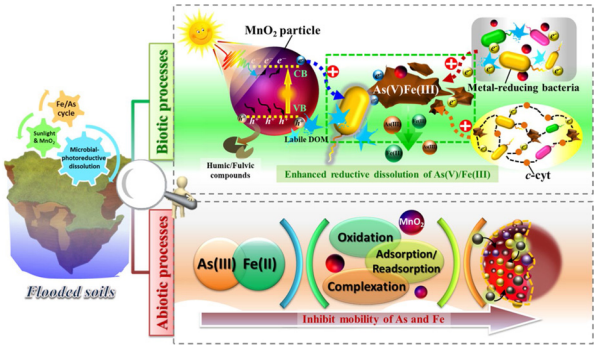

ARTICLE INFO

Editor: L. Eder

Keywords:
Flooded soils
Arsenic
Iron
Bioremediation
Manganese dioxide

ABSTRACT

This study examined the role of intermittent illumination/dark conditions coupled with MnO_2-ammendments to regulate the mobility of As and Fe in flooded arsenic-enriched soils. Addition of MnO_2 particles with intermittent illumination led to a pronounced increase in the reductive-dissolution of Fe(III) and As(V) from flooded soils compared to a corresponding dark treatments. A higher MnO_2 dosage (0.10 vs 0.02 g) demonstrated a greater effect. Over a 49-day incubation, maximum Fe concentrations mobilized from the flooded soils amended with 0.10 and 0.02 g MnO_2 particles were 2.39 and 1.85-fold higher than for non-amended soils under dark conditions. The corresponding maximum amounts of mobilized As were at least 92 % and 65 % higher than for non-amended soils under dark conditions, respectively. Scavenging of excited holes by soil humic/fulvic compounds increased mineral photoelectron production and boosted Fe(III)/As(V) reduction in MnO_2-amended, illuminated soils. Additionally, MnO_2 amendments shifted soil microbial community structure by enriching metal-reducing bacteria (e.g., *Anaeromyxobacter*, *Bacillus* and *Geobacter*) and increasing *c*-type cytochrome production. This microbial diversity response to MnO_2 amendment facilitated direct contact extracellular electron transfer processes, which further enhanced Fe/As reduction. Subsequently, the mobility of released Fe(II) and As(III) was

* Corresponding author at: School of Public Health and Management, Wenzhou Medical University, Wenzhou, 325035, People's Republic of China.
E-mail address: chenzheng_new@163.com (Z. Chen).

https://doi.org/10.1016/j.jhazmat.2020.123362
Received 28 April 2020; Received in revised form 10 June 2020; Accepted 29 June 2020
Available online 01 July 2020

partially attenuated by adsorption, oxidation, complexation and/or coprecipitation on active sites generated on MnO_2 surfaces during MnO_2 dissolution. These results illustrated the impact of a semiconducting MnO_2 mineral in regulating the biogeochemical cycles of As/Fe in soil and demonstrated the potential for MnO_2-based bioremediation strategies for arsenic-polluted soils.

1. Introduction

Arsenic (As) pollution derived from mine tailings is of worldwide concern as it severely deteriorates the quality of nearby farmland soil, as well as the safety of animals and residents in surrounding regions (Chen et al., 2018c; Liu et al., 2010; Xue et al., 2017). Under flooded (anoxic) conditions, the mobility of As is closely correlated with iron (Fe), both being released into soil solution by reductive dissolution of As(V)-Fe(III)-bearing minerals (Gorny et al., 2015; Qiao et al., 2019). The reductive dissolution is mainly driven by metal-reducing bacteria through extracellular electron transfer (EET) processes (Chen et al., 2017, 2016). These processes involve oxidation of labile organic substrates by metal-reducing bacteria for respiration and synchronous reduction of extracellular high-valence metal compounds to form an integrated respiratory chain (Shi et al., 2016). Hence, elucidating the behavior of As/Fe mobility in flooded, mine-tailing soils and the role microbial processes will enhance our comprehensive understanding of As/Fe biogeochemical cycling in natural environments.

Previous studies demonstrated that a variety of non-photosynthetic microorganisms harbor EET capabilities allowing electron exchange with extracellular minerals for their metabolism and survival in various environments (Chen et al., 2019a, b; Lu et al., 2012, 2014). Notably, many semiconducting minerals are photosensitive to visible light allowing production and migration of excited photoelectrons and holes from the conduction and valence bands of these minerals upon solar illumination (Lu et al., 2019; Xu and Schoonen, 2000). In some transitional zones of flooded soils, sunlight, microorganisms and semiconducting minerals are in intimate contact, and their interactions may alter biogeochemical transformation of both inorganic and organic compounds (Shi et al., 2016). Thus, electron interchange between semiconducting minerals, metal-reducing bacteria and sunlight could contribute to important and dynamic biogeochemical processes. Given that excited mineral photoelectrons are highly reductive and can trigger a series of redox reactions (Yang et al., 2011), it is highly plausible that intimately coupled microbial EET with semiconducting mineral derived photocatalysis could regulate the biogeochemical fate and transport of As/Fe in mine-tailing soils.

Semiconducting manganese dioxide (MnO_2) is an analogue for naturally existing pyrolusite (Darmane et al., 2008). It has gained considerable attention as a semiconductor material due to its high thermal stability, widespread abundance and outstanding photocatalysis capability (Chhabra et al., 2019; Kitchaev et al., 2017; Kumar et al., 2018). In particular, MnO_2 with its relatively narrow band gap (e.g., indirect band gap of α-MnO_2 is only 1.3 eV) displays enhanced performance for visible light absorption (Cockayne and Li, 2012), making it superior to several competing semiconductor materials (*e.g.,* titanium dioxide with a band gap of 3.2 eV can only absorb ultraviolet light with wavelengths < 387 nm) (Chen and Mao, 2007). Thus, photoelectrons generated from MnO_2 upon solar irradiation might theoretically participate in microbial EET processes, thereby increasing the electron flux delivered to extracellular electron acceptors. Considering pyrolusite is abundant in the surface soil layer that experiences close contact with microorganisms and sunlight, processes involving the intimate coupling of microbial EET with the photocatalysis properties of pyrolusite likely contribute to the reductive dissolution of As/Fe in sunlight illuminated flooded soils. A previous study confirmed that MnO_2 particles displayed a strong adsorption capability for Fe, but a relatively low ability to immobilize As (Lenoble et al., 2004). Thus, the underlying mobilization of As/Fe in MnO_2-amended soils is elusive as a number of potentially interconnected processes are likely involved in the complex biogeochemical environment of soil. Herein, the merits of a comprehensive examination to discern possible microbial mediation and abiotic reactions in MnO_2-amended soils are strongly warranted. Elucidating environmental controls upon biogeochemical mechanisms is highly important for targeting applications of MnO_2-based hybrid microbial-photoelectrochemical strategies for use in remediating As-polluted soils.

In this study, we selected MnO_2 particles as a model compound for pyrolusite to rigorously investigate the effects of combined MnO_2-derived photocatalysis with microbial EET processes on Fe/As mobilization in flooded arsenic-enriched soils formed on mine tailings. We further assessed mechanisms responsible for electron exchanges/transport involving MnO_2 particle stimulation of soil microbial diversity and dissolved organic matter bioavailability. Results of this study will inform basic and applied research targeting MnO_2-based hybrid microbial-photoelectrochemical technologies for remediation of arsenic-polluted soils.

2. Materials and methods

2.1. Soil sampling and MnO_2 characterization

Arsenic-enriched soils were sampled from abandoned farmland (20–30 cm depth below the surface) located near a realgar (α-As_4S_4) mine-tailing site in Heshan Village, Changde City, Hunan Province, China (Chen et al., 2018c). Samples were stored at 4 °C before a subsample was gently crushed, sieved (2-mm screen) and homogenized for subsequent use. Another subsample was passed through a 0.16-mm screen for elemental and mineralogical characterization. Detailed methods for elemental analysis are summarized in Method S1 of supplemental materials. The soil contained 30.8 ± 2.9 g/kg total iron and 507 ± 98 mg/kg total arsenic (Table S1). Analysis of representative crystalline compounds indicated predominantly oxidized states for both As and Fe (Fe(III) & As(V), shown in Fig. S1).

2.2. Soil microcosm experiments

To evaluate the mobilization/speciation changes of As and Fe in response to the addition of MnO_2 particles, batch anoxic microcosms were conducted in parallel for two illumination conditions (i.e., intermittent illumination and dark conditions). The MnO_2 particles were purchased from Aladdin (USA). The morphology and crystalline structure of MnO_2 particles (1 − 50 μm) were identified by scanning electron microscopy (SEM) and X-ray powder diffraction (XRD) (Fig. S2a and 2b). Each treatment was carried out in triplicate in 105-mL serum bottles at 30 °C. Briefly, each experimental microcosm was incubated with 12.0 g tailing soils, 36.0 mL of 30.0 mM sodium acetate (NaAc) solution, and 0.02 or 0.10 g MnO_2 particles. A series of control treatments containing no MnO_2 amendment was incubated under respective illuminated/dark conditions. Under intermittent illumination, soil microcosms were incubated using a 12-h day/night cycle with simulated sunlight (50 μmol/m^2·s from white LED lamp). Light energy surrounding the microcosm was measured using a light energy meter (Diving-PAM, WALZ, Germany). After purging oxygen with high purity nitrogen for 1.0 h in the liquid phase and another 0.5 h in the headspace, all microcosms were sealed with butyl rubber stoppers and aluminum caps before transfer to an incubator. Additionally, a batch of abiotic microcosms was incubated under parallel conditions, but using

sterilized soils and NaAc solutions (sterilized by autoclaving at 120 °C for 20 min). A detailed experimental design is provided in Table S2.

2.3. Assays for adsorption and speciation transformations of As and Fe

Considering adsorption of As and Fe by MnO_2 particles (Nishimura and Umetsu, 2001), the mobility of As and Fe from flooded soils is altered. Herein, we conducted two assays to assess As and Fe sorption dynamics with MnO_2 particles. In the first assay, sorption was determined by reacting 0.02 or 0.10 g of MnO_2 particles and 36.0 mL gradient concentrations of As(V), As(III), Fe(III) or Fe(II) in 50-mL centrifuge tubes (detailed procedures reported in Method S2). Samples were shaken at 200 rpm and 30 °C for 24 h. At the end of the reaction period, As and Fe in the solution were subjected to qualitative and quantitative analyses to determine the effect of MnO_2 particles on adsorption and speciation changes of As and Fe.

In the second assay, 0.02 or 0.10 g of MnO_2 particles and 4.0 mL of soil extracted dissolved organic matter (containing 352 ± 21 mg/L of TOC) were sealed in a semi-permeable dialysis bag (molecular weight cutoff: 500 Daltons) that enables the exchange of released metal ions and electrons but prevents the penetration of MnO_2 particles and high-molecular-weight DOM. DOM for the dialysis bags was extracted from freeze-dried soils using Milli-Q water with a ratio of 1:3 (weight: volume) while stirring at 200 rpm for 48 h at 20 °C in the dark. The sealed semi-permeable dialysis bags were placed on the soil and incubated in the same anoxic microcosms as described in Section 2.2 (Fig. S3). At the end of the incubation period, we separated the sealed MnO_2 particles for acid digestion to (1) quantify adsorbed As and Fe and (2) determine the speciation of adsorbed As/Fe by XPS (Quatum-2000, USA).

2.4. Analytical methods

2.4.1. Quantification of released arsenic, iron and manganese

Concentrations of dissolved Fe(II), Fe(T) (total iron), As(III) and As (T) (total arsenic) in supernatants were determined for each soil microcosm. Prior to measurement, ~2.0 mL of supernatant was filtered through a sterile 0.22-μm filter (polyethersulfone, Jinteng Co., Ltd, China). Dissolved Fe(II) and Fe(T) were quantified using a ferrozine assay as previously described (Chen et al., 2018c). Dissolved As(III) and As(T) were quantified using HPLC-AFS (Titan, SA-50, China) and ICP-Mass Spectrometry (NexION 2000, PerkinElmer, USA), respectively (Chen et al., 2016; Farías et al., 2015). All operations mentioned above were conducted in an anaerobic glovebox. To determine Mn(T) (total manganese) concentration, ~1.0 mL of supernatant from each microcosm was filtered through a sterile aforementioned filter and acidized using nitric acid (wt%: 65 %). The concentration of released Mn(T) was detected using flame atomic absorption spectrometry (Shimadzu, AA-6880, Japan) (Sachdev et al., 1967).

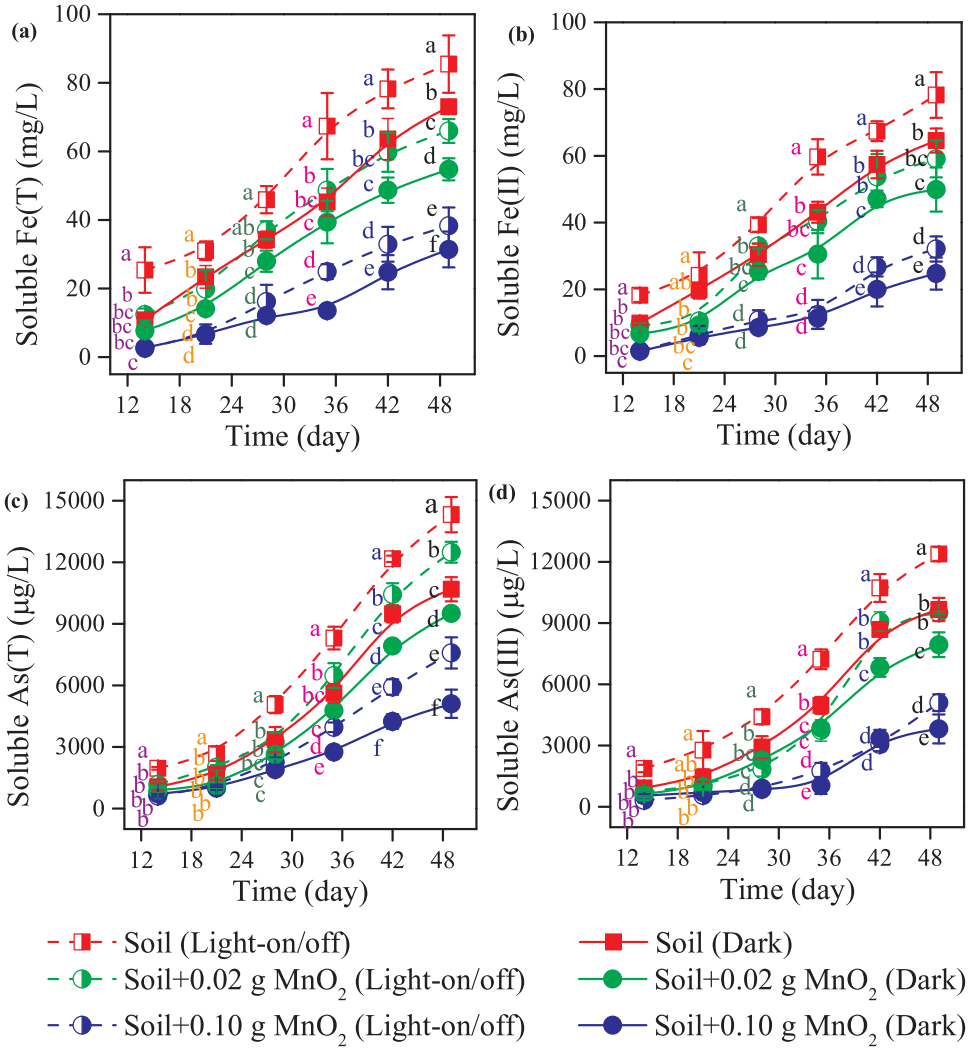

Fig. 1. Concentrations of soluble Fe(T) (a), Fe(II) (b), As(T) (c) and As(III) (d) released from anaerobic soil microcosms amended with 0.02 and 0.10 g MnO_2 particles under dark and intermittent illumination conditions (mean ± SD, n = 3). Note: Different lowercase letters within experimental groups indicate significant differences at $P < 0.05$.

2.4.2. Analysis of dissolved organic carbon

In soil microcosms, dissolved organic matter (DOM) plays several important roles in controlling metal mobility (Han et al., 2016). On the one hand, labile DOC fractions, like low-molecular-weight sugars, organic acids and amino acids, serve as important electron donors through microbial metabolism to supply bio-electrons which are subsequently transferred to high valence metals, promoting the reductive dissolution of metal from soil (Chen et al., 2018b). On the other hand, high-molecular-weight organic carbon compounds, such as humic and fulvic acid like-compounds, are considered as a capture agent for photoholes, suppressing the recombination of electron-hole pairs (Chen et al., 2019a). Thus, we analyzed (1) DOC derived from the soil and liquid phases (abbreviated as SDOC and LDOC, respectively) of the microcosms, and (2) changes in the fluorescence intensities of high-molecular-weight humic and fulvic acid-like compounds. SDOC was extracted from a mixture of 2.0 g freeze-dried soil and 20.0 mL-Milli-Q water shaken at 200 rpm and 25 °C for 24 h in the dark (Xu et al., 2013). LDOC and SDOC supernatants were passed through a pre-combusted GF/F filter (Whatman, UK) before quantification using a TOC analyzer (Shimadzu, TOC-L CPH, Japan). The abundances of fulvic and humic acid-like compounds in SDOC extracts were estimated from their respective fluorescence intensities at 451 and 464 nm, respectively, following excitation at 279 nm using a fluorescence spectrophotometer (FS5, Edinburgh, UK) (Koo et al., 2017).

2.4.3. Determination of c-type cytochromes

Outer-membrane *c*-type cytochromes (*c*-cyts) of microorganisms play a critical role in EET processes, which could provide rapid electron transfer via direct contact with *c*-cyts and electron acceptors (Liu et al., 2015; Richardson et al., 2012). To compare *c*-cyts production, a 0.5-g soil sample from each treatment cultured for 49 days and 1.0 mL 0.01 M PBS solution were mixed in a 2.0-mL sterilized centrifuge tube and then manually homogenized for 3 min. The resulting mixtures were centrifuged at 3000 rpm for 15 min to separate the supernatant. Production of *c*-cyts was determined according manufacturer's protocols for the *c*-cyt ELISA Kit (Shanghai Lanpai Biotechnology, China) (Jin et al., 2019). Optical density (O.D.) values at 450 nm were recorded within 15 min using a microtiter plate reader (PerkinElmer, EnSpire, USA). Finally, *c*-cyts concentration was quantified according to the standard curve for *c*-cyts concentration versus O.D. values.

2.4.4. High-throughput sequencing

The 0.5-g soil samples derived from the 49-day microcosms of all treatments were collected for total DNA extraction. DNA extraction followed protocols for the Fast DNA Spin Kit for Soil (MP Biomedical, USA). To assess the composition of microbial communities, extracted total DNA was subjected to high throughput sequencing. In the high-throughput sequencing process, the 338 F and 806R primers were used to amplify the bacterial V4-V5 region of 16S rRNA genes by PCR (Chen et al., 2017). PCR products were pooled into 2% agarose gels for electrophoresis. The resulting products were purified using an AxyPrep DNA Gel Extraction Kit (Axygen Biosciences, USA) and quantified using a QuantiFluor™-ST Kit (Promega, USA). The purified amplicons were pooled at equal molar concentrations, and paired-end sequencing (2 × 250) was conducted on an Illumina MiSeq platform. The 16S rRNA gene sequence data were processed using the QIIME 1.8.0 tool kit. Detailed information regarding the sequencing analysis is given in Method S3.

2.5. Statistical analysis

We assessed treatment differences by analysis of variance in conjunction with the least significant difference test at a significance level of $P < 0.05$ using SPSS 20.0. Weighted UniFrac principal coordinate analysis (PCoA) of the potentially active bacterial community and redundancy analysis (RDA) were performed using CANOCO 4.5 to assess differences in community composition and correlations between key functional microbial members and environmental variables.

3. Results and discussion

3.1. Release of As(III) and Fe(II) from flooded soils

Over the 49-day incubation period, very limited amounts Fe(T) and As(T) (less than 0 ~ 0.5 mg/L and 100 ~ 700 μg/L) were released from abiotic (i.e., sterilized) assays (Fig. S4). In contrast, Fe(T) and Fe(II) mobilization in non-sterile (biotic) treatments gradually increased with greater incubation time, with concentrations of released Fe(II) and Fe (T) being similar (Fig. 1a-b). These results indicated that microbial activities played an important role in the reductive dissolution of Fe (III). Importantly, Fe(III) dissolution was promoted by intermittent illumination compared to dark conditions. We attributed this response to enhanced production of photoelectrons originating from the illuminated endogenous minerals that then flowed into microbial extracellular electron transfer chains (Chen et al., 2019b). MnO_2-ammended soils showed a sharp decrease in reductive dissolution of Fe(III) and demonstrated a dose-dependent response. At the end of the 49-day incubation period, maximum Fe(II) concentrations released from MnO_2-ammended soils under intermittent illumination were 66.0 ± 6.5 (0.02 g) and 38.3 ± 5.3 mg/L (0.10 g) (Fig. 1b). These maximum values were only 77 and 44 percent that of their respective control groups under the same illumination conditions. Therefore, MnO_2 amendment decreased the mobility of released Fe(II).

Intermittent illumination resulted in higher As(V) reductive dissolution than for dark conditions under biotic conditions, regardless of supplementation with MnO_2 particles (Fig. 1c and d). MnO_2 particles produced an inhibitory effect on As mobility under illuminated conditions in comparison to their respective control groups (Fig. 1c and d). In general, average concentrations of As(T) and As(III) followed the order: soil (intermittent illumination) > soil + 0.02 g MnO_2 (intermittent illumination) > soil (dark) > soil + 0.02 g MnO_2 (dark) > soil + 0.10 g MnO_2 (intermittent illumination) > soil + 0.10 g MnO_2 (dark). As the dosage of MnO_2 particles increased from 0.02 to 0.10 g, maximum As (III) concentrations decreased from 9498 ± 65–5202 ± 412 μg/L and 7938 ± 605–3816 ± 708 μg/L under intermittent illumination and dark conditions, respectively (Fig. 1d). These As(III) values were significantly lower than that of the illuminated control (12383 ± 337 μg/L) and dark control (9667 ± 570 μg/L) groups. Notably, the fraction of As(III) to As(T) released from MnO_2-supplemented assays was lower than for their corresponding control groups. At the end of the 49-day incubation, the As(III) fraction released from the illuminated and dark control groups were 87 % and 91 %. In contrast, the associated fractions for the 0.02 and 0.10 g MnO_2-amended assays were 83 % and 75 % under dark conditions, whereas corresponding fractions were 76 % and 67 % under intermittent illumination. These results revealed that a portion of the released As(III) originated from oxidation by MnO_2 particles (Chen et al., 2018a; Xiong et al., 2017), particularly at higher MnO_2 doses. The discrepancy in As(III) to As(T) fractions across all amendments might be attributed to the differential adsorption capability of MnO_2 for As and Fe and also to associated redox reactions induced by MnO_2 particles (Ma et al., 2020). The involved mechanisms were further discussed in the following sections.

3.2. Quantification and speciation of adsorbed As and Fe on MnO_2 particles

We further investigated the effects of MnO_2 particles on As and Fe adsorption and species transformations by conducting adsorption experiments (Tables S3–S6). In agreement with the above-mentioned results, MnO_2 demonstrated a weaker adsorption efficiency for As(III)/As(V) (< 90 % adsorption efficiency for 2000 μg/L with 0.10 g MnO_2) compared to that for Fe(II)/Fe(III) (nearly 100 % for 20 mg/L at 0.10 g MnO_2). The higher sorption affinity for Fe(II)/Fe(III) occurred even though Fe concentrations were at least an order of magnitude higher

than those of As(III)/As(V). These differences in adsorption affinities might be ascribed to electrostatic repulsion between negatively charged MnO_2 particles and arsenite/arsenate oxyanions (Crimi and Ko, 2009) or to competitive adsorption between As and Fe (Thanh et al., 2012). The competitive adsorption interpretation is supported by results from subsequent sorption assays with coexisting As and Fe concentrations (Table S7). Notably, MnO_2 contains intermediate valency Mn(IV), which is capable of oxidizing Fe(II) and As(III) into Fe(III) and As(V), but is not able to reduce Fe(III) and As(V) (Table S4 and Table S6). These mechanisms are attributed to a higher oxidation potential (E_o') for MnO_2 than that of AsO_4^{3-} and Fe^{3+}, which is described by the following reactions:

$$2H^+ + AsO_3^{3-} + MnO_{2(S)} \rightarrow Mn^{2+} + AsO_4^{3-} + H_2O \quad (1)$$

$$4H^+ + 2Fe^{2+} + MnO_{2(S)} \rightarrow Mn^{2+} + 2Fe^{3+} + 2H_2O \quad (2)$$

The MnO_2 particles contained within the dialysis bags were subjected to acid digestion for quantification of adsorbed As and Fe. Concurrently, we determined As(T) and Fe(T) concentrations contained in the liquid phase and dialysis bags. The total masses of As and Fe in the solution (liquid + dialysis) and solid (sorbed to MnO_2) phases were used to calculate the mass of As/Fe mobilized from each amendment (Formulas S1-S2 of supplemental materials). Treatments with MnO_2 particles under intermittent illumination resulted in higher mobilization of As and Fe than other treatments (Fig. 2). At the end of the incubation period (day 49), the total amounts of Fe mobilized from illuminated soils amended with 0.02 and 0.10 g MnO_2 particle were 1.85 and 2.39-fold greater than non-amended soil under dark conditions (Fig. 2a); As mobilization was 1.65 and 1.92-fold greater for illuminated + MnO_2 amended soil versus dark, non-amended soil (Fig. 2b). These results indicated that addition of MnO_2 particles, particularly under intermittent illumination, significantly promoted mobilization of As/Fe from flooded soils.

To identify the existence and speciation of As and Fe adsorbed onto MnO_2 particles, MnO_2 particles were separated for TEM observation and XPS analysis. TEM-EDS mapping provided direct evidence for sorption of As and Fe on MnO_2 surfaces (Fig. 3a). The chemical states and corresponding contents of adsorbed As, Fe, Mn and O were examined by XPS analysis (Fig. 3b–e). In terms of content and valence changes for these elements, nearly 87.9 % and 88.1 % of As(T) and Fe (T) were presented as As(V) and Fe(III) after MnO_2 adsorption (Table S7), indicating that MnO_2 promoted oxidation of the released As(III) and Fe(II). In the As 3d spectrum, a pair of representative peaks for As (V) and As(III) were located at 45.7 and 44.8 eV (Ma et al., 2020) and indicated a greater sorption of As(V) than As(III) on MnO_2 particles (Fig. 3b). Further, the larger integral area for the fitted peak of Fe(III) than Fe(II) (709.0 and 710.8 eV in the Fe 2p spectrum, respectively (Biesinger et al., 2010)) demonstrated that much of the adsorbed Fe(II) was oxidized to Fe(III) (Fig. 3c). The distributions of Mn(II), Mn(IV) and Mn(III) with the binding energies at 644.2, 643.4 and 643.1 eV were depicted in the Mn 2p spectrum (Xiong et al., 2017). These results indicated that a transitional Mn(III) species was produced during redox reactions of Mn(IV)/Mn(II) (Fig. 3d). Finally, the three overlapping peaks in the O 1s spectrum were assigned to functional groups of adsorbed water (H_2O), hydroxyl (−OH) and lattice oxygen (O^{2-}) (532.84, 531.72 and 529.60 eV, respectively (Biesinger et al., 2010)) (Fig. 3e). In particular, the high proportion of O_2^- and −OH moieties (20.4 and 51.5 percent) in oxygen-bearing groups (shown in Table S7) provided evidence for more active sites available for subsequent adsorption and/or complexation between released Mn(II) and As(V)/Fe (II). Thus, the O 1s spectrum suggested that binary oxide and hydroxyl groups were formed in the mineral phase during As and Fe adsorption to MnO_2 particles.

Concentrations of released Mn(T) did not increase in MnO_2-amended assays (Fig. S5), even though greater amounts of As(V) and Fe (III) might be expected to promote reductive dissolution of MnO_2. Rather, the concentration of released Mn(T) was perceived to decreased at higher dosages of MnO_2 particles under selected conditions. This phenomenon might be attributed to adsorption of Mn(II) following reductive dissolution as it is easily complexed with adsorbed Fe(III) (Li et al., 2019a). Similarly, multi-step As(III) adsorption with adsorbed Fe (III) and Mn(II) might form As(V)/Fe(III)/Mn(II)-complexes via oxidation of As(III) to As(V) during the reductive dissolution of MnO_2 particles (Nishimura and Umetsu, 2001; Ociński et al., 2016). Therein, the mechanism regarding As(III) oxidation/adsorption resulting from dynamic Fe(II) oxidation-adsorption/readsorption of Fe(III) under anaerobic conditions merits further investigation. Nevertheless, our results clearly indicated that MnO_2 particles stimulated reductive dissolution of As(V)/Fe(III) from flooded soils and subsequently suppressed the mobility of released As(III) and Fe(II) due to rapid adsorption/oxidation on MnO_2 particles.

3.3. Regulation of microbial DOC consumption by MnO_2 particles

Microorganisms assimilate low-molecular-weight DOC (e.g., labile acetate) for their extracellular respiration and synchronously produce bio-electrons (Chen et al., 2018b; Liu et al., 2018). In general, the removal of LDOC and SDOC is a proxy for microbial consumption of DOC in our microcosms. The utilization of LDOC followed a similar trend with that of SDOC among all treatments (Fig. 4a-4b). After incubating for 35 days, DOC loss from intermittently illuminated microcosms was lower than for microcosms incubated in the dark. This indicated that dark condition promoted microbial DOC consumption. Different doses of MnO_2 particles also induced a differential impact on DOC loss in illuminated versus dark conditions. Specifically, DOC loss increased as the dosages of MnO_2 particles increased under dark conditions, whereas DOC loss was decreased with increasing MnO_2 dosages under intermittent illumination. When comparing the 0.02 versus 0.10 g MnO_2-ammendments under dark conditions, the utilization efficiencies for

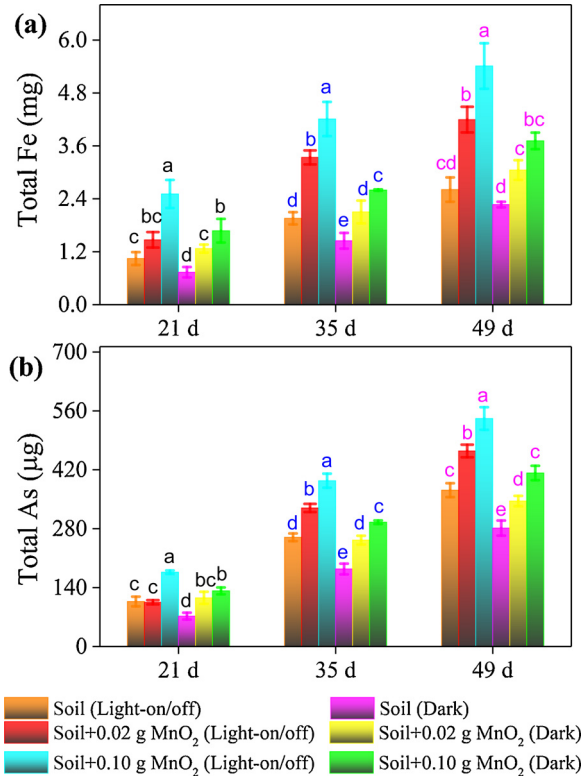

Fig. 2. Total amounts of Fe (a) and As (b) released in experimental assays using semi-permeable dialysis bags (mean ± SD, n = 3). Note: Different lowercase letters within experimental groups indicate significant differences at $P < 0.05$.

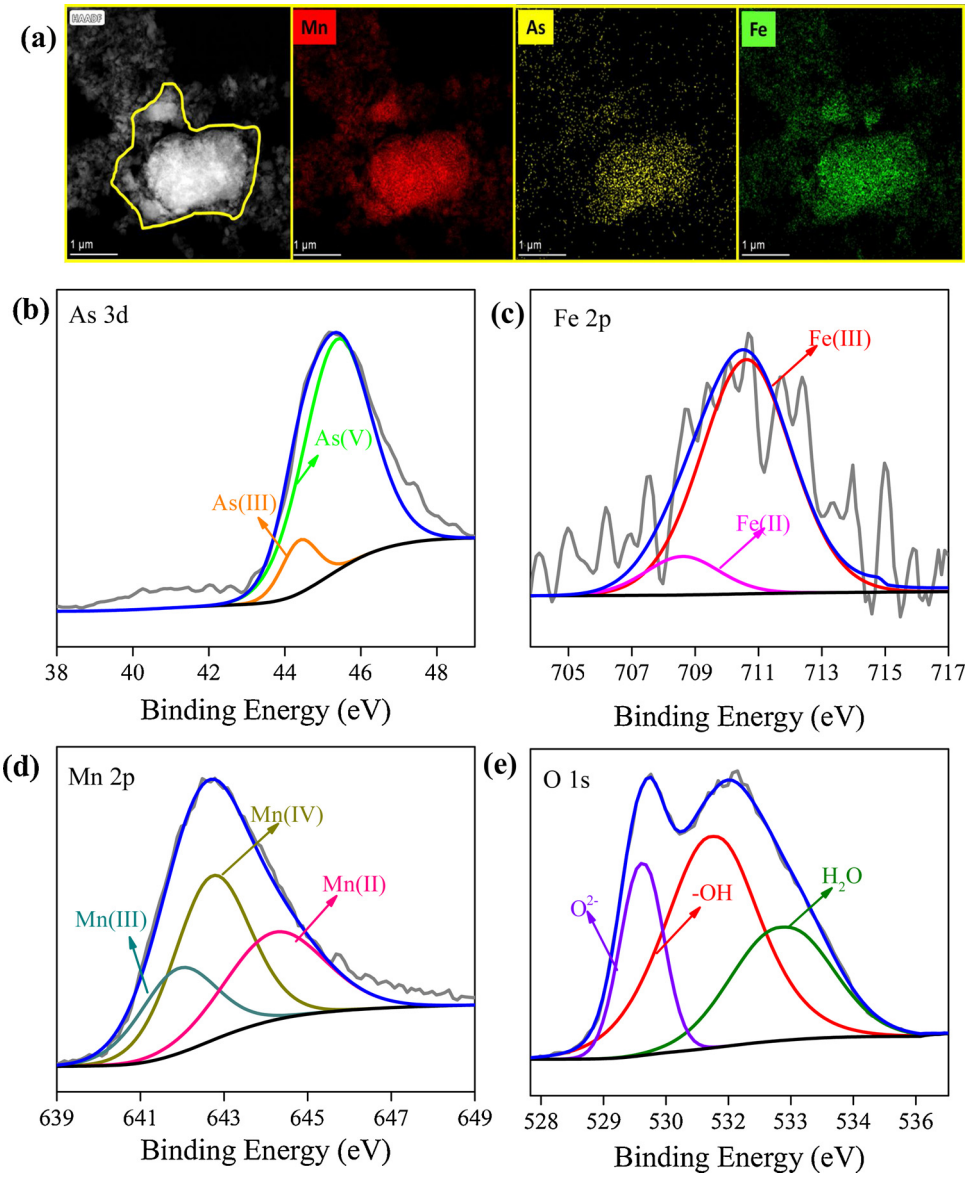

Fig. 3. TEM morphology (a) of MnO_2 particles separated from dialysis bag and corresponding EDS maps of Mn, As and Fe distribution. XPS spectra showing speciation of adsorbed As (b) Fe (c), Mn (d) and O (e) on separated particles.

LDOC and SDOC of the 0.10 g MnO_2-treatment on the 49th day were 8.4 and 6.3 % higher, respectively. This implied that supplementation with greater doses of MnO_2 particles stimulated a higher consumption of DOC for supplying greater amounts of bio-electrons under dark conditions. Notably, we found higher reductive dissolution of As(V)/Fe (III) with greater dosages of MnO_2 particles under dark conditions (Fig. 2). This implied that As/Fe reduction in dark conditions could be boosted through adding greater dosages of MnO_2 particles to stimulate microbial production of bio-electrons.

Although lower DOC consumption occurred at greater MnO_2 dosages under intermittent illumination, the corresponding reductive dissolution of As(V)/Fe(III) was distinctly higher at greater MnO_2 dosages (Fig. 2). Thus, we inferred that a greater amount of photoelectrons excited from exogenous semiconducting MnO_2 particles were supplied to promote the higher reductive dissolution of As(V)/Fe(III) in the intermittently illuminated assays (Chen et al., 2019b). Additional evidence for this supposition resulted from a greater decline of fluorescence signals, corresponding to the heavy-molecular-weight humic/fulvic acids-like compounds, in the intermittent illumination versus dark treatments (Fig. 4c). Particularly, the loss of fulvic/humic acids-like compounds caused by intermittent illumination was magnified in the presence of greater dosages of MnO_2 particles. Thus, these results suggested that photoelectron-hole recombination was effectively hindered as a greater number of holes were quenched by fulvic/humic acids. This allowed for a hopping migration of photoelectrons, which subsequently fed into the microbial extracellular respiratory electron transfer chain. Hence, the more pronounced As/Fe reductive dissolution stimulated by MnO_2 particles in intermittently illuminated assays was resulted from enhanced photoelectron production from the MnO_2-amended soils under intermittent illumination.

3.4. Stimulation of *c*-cyts production by MnO_2 particles

Although MnO_2 particles display outstanding visible light-driven photocatalysis capability, the mechanisms underlying the production of *c*-cyts at the molecular level remain relatively unexplored. Our results indicated a dose-dependent effect of MnO_2 particles on *c*-cyts production, where higher *c*-cyts production resulted from greater MnO_2 dosages, regardless of light illumination (Fig. 5). Increased production of *c*-cyts derived from the addition of 0.02 and 0.10 g MnO_2 particles were

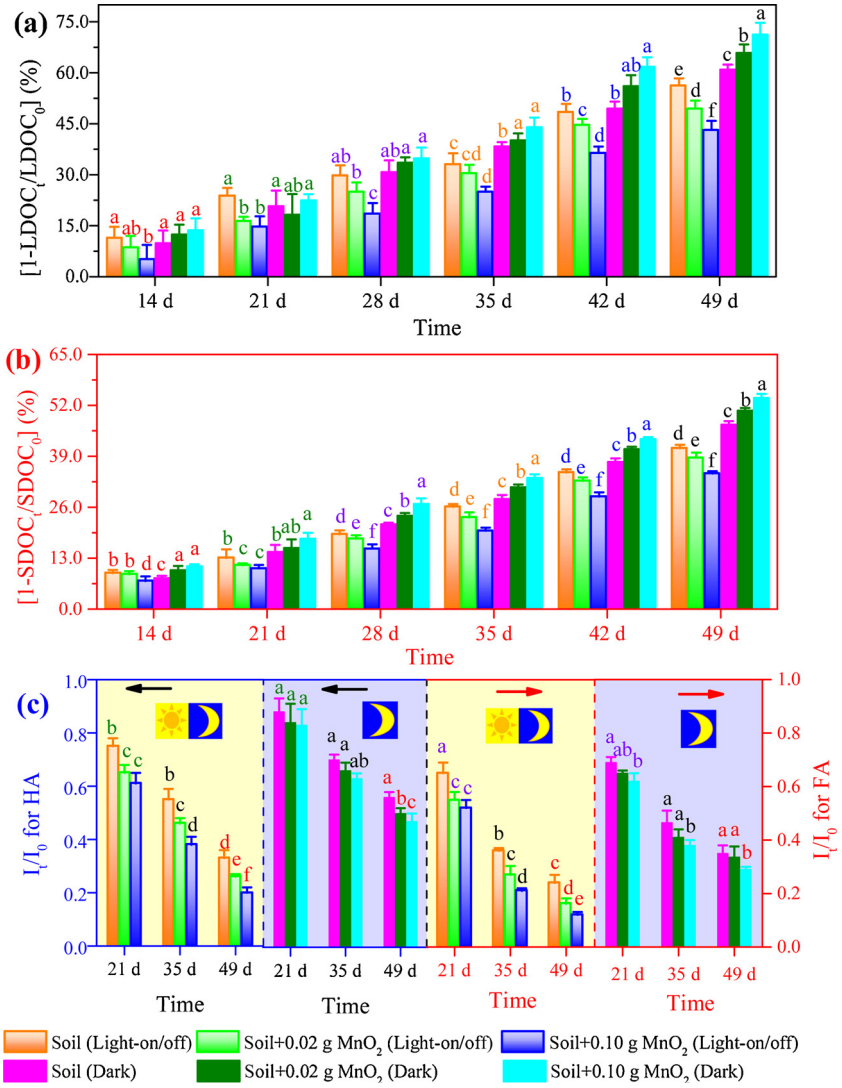

Fig. 4. Utilization of dissolved organic carbon derived from liquid (a) and soil phases (b) and the ratio representing the change of fluorescence intensities of HA and FA in comparison to that of the initial incubation samples in soil phase (c) (mean ± SD, n = 3). HA, FA, I_0 and I_t refer to humic- and fulvic-acid like compounds, and intensities of fluorescence emissions from the initial incubation and various sampling times, respectively. Note: Different lowercase letters within experimental groups indicate significant differences at $P < 0.05$.

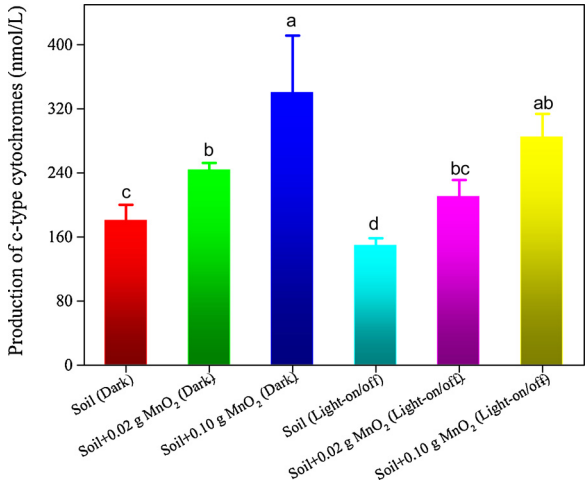

Fig. 5. Production of *c*-type cytochromes in each amendment after a 49-day incubation (mean ± SD, n = 3). Note: Different lowercase letters indicate significant differences at $P < 0.05$.

nearly 1.9 and 1.3-fold of that of non-MnO_2 amended assays under dark conditions. Additionally, previous findings demonstrated that a nearly 14-fold expression of *omcS* (a gene encoding specific *c*-cyt OmcS) in *Geobacter* was up-regulated in the presence of Mn(IV) oxide (Aklujkar et al., 2013). Our results are consistent with these previous findings. Because outer-membrane *c*-cyts contain several iron porphyrins or hemes that are responsible for electron transport (Wang et al., 2019), higher production of *c*-cyts will inevitably lead to more extracellular electron transport across *c*-cyts of microbes to extracellular electron acceptors (Hernandez and Newman, 2001; Reguera et al., 2005). Such behavior is particularly important to EET processes involving the direct contact between metal-reducing bacteria that possess electrically conductive pili (e.g., *Geobacter* and *Shewanella*) and extracellular Fe(III)/As (V) via microbial nanowires (Chen et al., 2019c; Gorby et al., 2006; Li et al., 2019b). Therefore, our results identified a mechanism by which MnO_2 particles promoted a direct contact based EET process by stimulating more *c*-cyts production in the soil microbial community.

3.5. Microbial community composition

High-throughput sequencing results revealed that the predominant

bacterial phyla belonged to *Firmicutes* (43–67 %), *Proteobacteria* (11–24 %), *Bacteroidetes* (4–17 %) and *Acidobacteria* (2–5 %) (Fig. 6a). Compared to dark conditions, intermittent illumination resulted in an increased abundance of *Bacteroidetes* (4–17 %), whereas it led to a decrease of *Proteobacteria* (14–25 %). For MnO_2-amended treatments, abundances of several representative phyla (e.g., *Proteobacteria*, *Bacteroidetes* and *Acidobacteria*) either increased or decreased in response to increased MnO_2 dosages under a given illuminated condition. In terms of general members, MnO_2 amendments resulted in a pronounced increase to abundances of *Geobacter* (13–20 %), *Bacillus* (4–9 %) and *Clostridium* (4–8 %) in contrast to their respective control groups under corresponding illumination conditions (Fig. 6b). Especially, the abundance of *Geobacter*, a genus that generally assembles electrically conductive *c*-cyts (Liu et al., 2015), was markedly increased as the MnO_2 dosages increased of under both illuminated and dark conditions. We further calculated total abundances for eight representative genera known to be responsible for the reduction of high valence metal compounds via the EET process (Table 1) (Chen et al., 2017; Qiao et al., 2018a, b). This result confirmed a higher abundance of metal-reducing bacteria in MnO_2-amended soils, particularly in those supplemented with greater MnO_2 dosages. These findings demonstrated that the combination of intermittent illumination and MnO_2 amendment altered the microbial community structure of flooded soils by enriching metal-reducing bacteria.

The changes in bacterial communities regulated by MnO_2 and/or illumination were further investigated using PCoA based on the weighted Fast UniFrac metric (Fig. 7a). Principal axis 1 of the PCoA matrix contained 51.7 % of the variation among sample positions. The positions corresponding to microbial communities with the same dosage of MnO_2 particles were closely associated. The closely overlapping positions between intermittent illumination and dark treatments receiving 0.10 g MnO_2 particles indicated a close similarity in microbial communities, suggesting that MnO_2 is a more important driver than illumination condition in shaping microbial communities.

We further employed RDA to assess correlations between bacterial genera and Fe/As mobilization (Fig. 7b). The main metal-reducing members (e.g., *Bacillus*, *Anaeromyxobacter*, *Desulfitobacterium* and *Thermincola*) were positively correlated with the mobility of As and Fe from flooded soils. For the intermittent illumination + MnO_2 amendment, sharp angles occurred between the corresponding centrifugal lines derived from genera variables (e.g., *Bacillus*, *Anaeromyxobacter* and *Pseudomonas*) and environmental variables (e.g., mobility of Fe and As). This pattern revealed that the activities of these bacteria were positively correlated to the reductive dissolution of Fe/As under such combined treatment. In contrast, for MnO_2-amended soils under dark conditions, the abundance of *Thermincola* was negatively correlated with the mobility of As and Fe, but was positively correlated with loss of LDOC and SDOC. Moreover, positive correlations were observed among

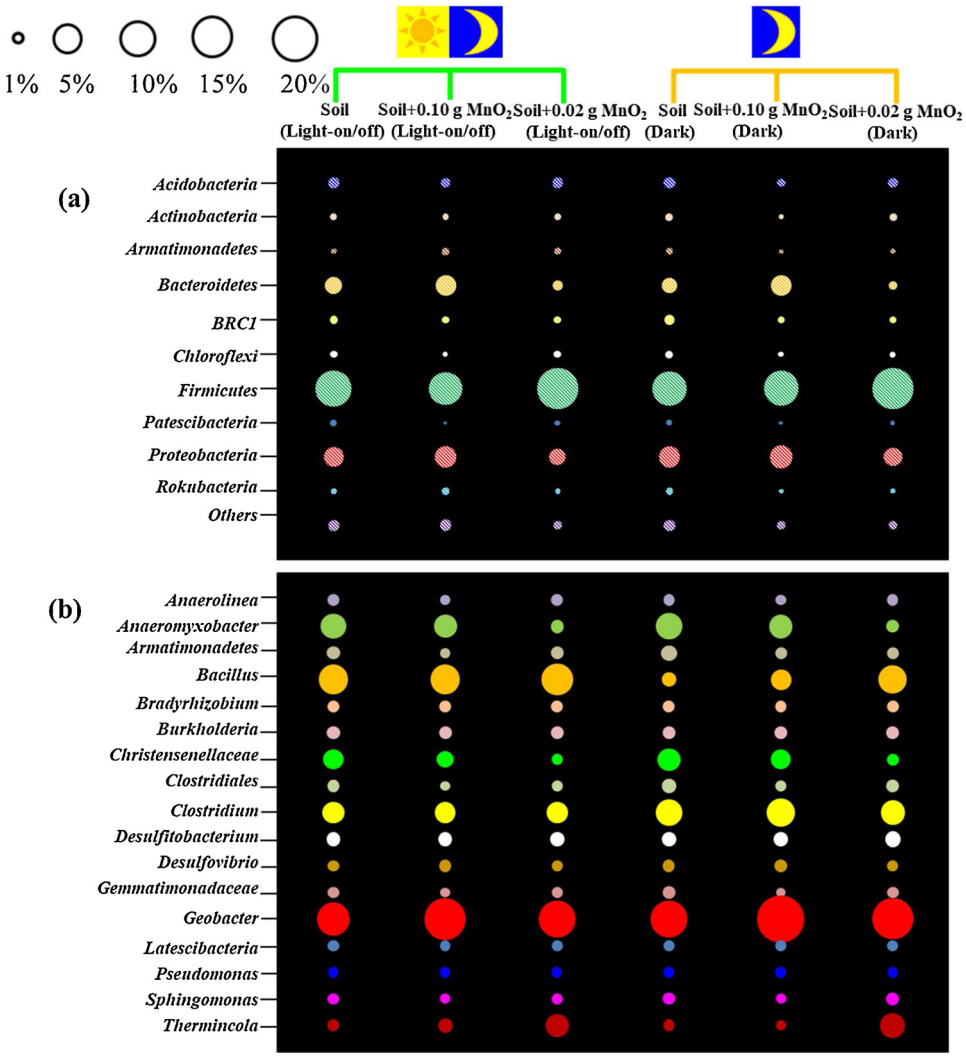

Fig. 6. Relative abundance of potentially active bacterial community at phylum (a) and genus (b) levels in respective amendments. Only those microbial members with an abundance greater than 1% are displayed.

Table 1
Relative abundance (%) of metal-reducing bacteria for each amendment after a 49-day incubation (mean ± SD, n = 3).

Genera	Soil (Light-on/off)	Soil + 0.02 g MnO_2 (Light-on/off)	Soil + 0.10 g MnO_2 (Light-on/off)	Soil (Dark)	Soil + 0.02 g MnO_2 (Dark)	Soil + 0.10 g MnO_2 (Dark)
Anaeromyxobacter	5.7 ± 0.4^{a}	1.6 ± 0.3^{c}	4.9 ± 0.3^{b}	6.3 ± 0.6^{a}	1.5 ± 0.4^{c}	5.0 ± 0.4^{ab}
Bacillus	8.1 ± 0.4^{b}	9.1 ± 0.1^{a}	8.0 ± 0.1^{b}	1.8 ± 0.8^{d}	7.4 ± 1.0^{bc}	3.8 ± 1.1^{c}
Clostridium	4.2 ± 0.2^{c}	4.0 ± 1.1^{c}	4.0 ± 0.8^{c}	6.1 ± 0.4^{ab}	5.3 ± 0.9^{b}	7.5 ± 1.3^{a}
Desulfitobacterium	1.1 ± 0.1^{d}	2.0 ± 0.1^{b}	1.8 ± 0.2^{bc}	1.9 ± 0.1^{b}	2.3 ± 0.1^{a}	1.8 ± 0.0^{c}
Desulfovibrio	1.3 ± 0.0^{b}	1.2 ± 0.0^{c}	1.4 ± 0.0^{a}	1.3 ± 0.0^{b}	1.2 ± 0.1^{c}	1.4 ± 0.1^{a}
Geobacter	9.9 ± 0.9^{d}	12.5 ± 0.5^{c}	14.9 ± 1.4^{b}	12.3 ± 0.4^{c}	15.3 ± 0.7^{b}	20.3 ± 2.0^{a}
Pseudomonas	1.0 ± 0.0^{a}	1.0 ± 0.2^{a}	1.0 ± 0.0^{a}	1.0 ± 0.0^{a}	1.0 ± 0.0^{a}	1.0 ± 0.0^{a}
Thermincola	1.3 ± 0.0^{b}	5.0 ± 1.1^{a}	1.9 ± 0.1^{b}	1.3 ± 0.1^{b}	5.5 ± 0.4^{a}	1.0 ± 0.1^{c}
Total	32.4 ± 1.2^{c}	35.9 ± 3.1^{bc}	37.9 ± 2.8^{b}	31.9 ± 2.4^{c}	39.4 ± 3.3^{ab}	42.4 ± 4.1^{a}

Note: Different lowercase letters within each row indicate significant differences at $P < 0.05$.

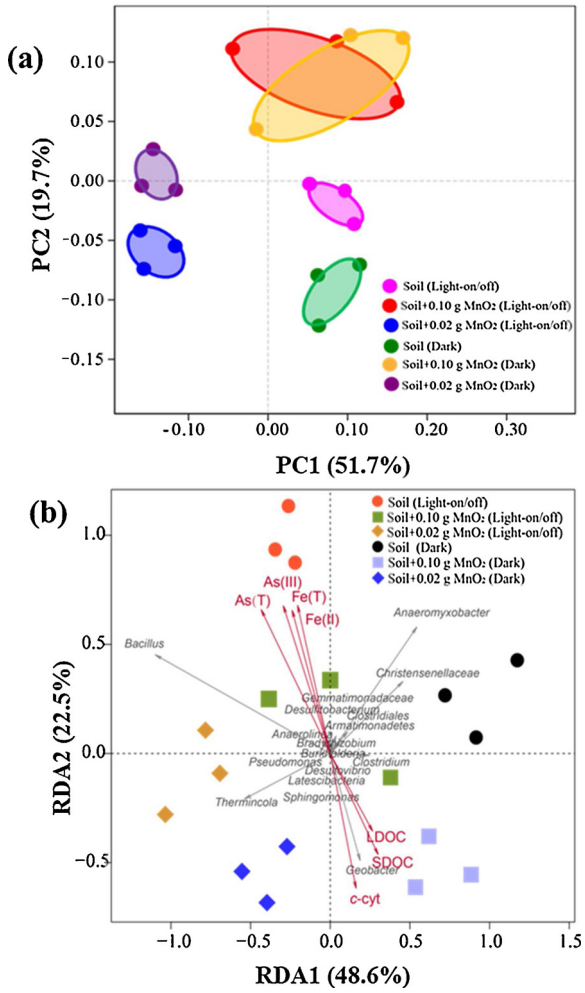

Fig. 7. PCoA of microbial diversity based on Operational Taxonomic Units using the weighted Fast UniFrac metric (a) and RDA based on relationships between key genera and environmental variables (b).

c-cyts production, abundance of *Geobacter* and DOC loss, suggesting that DOC bioavailability and enrichment of *Geobacter* were associated with enhanced production of *c*-cyts. Overall, these results highlighted important relationships between microbial diversity and environmental factors in response to semiconducting minerals and illumination conditions in flooded arsenic-enriched soils.

3.6. Environmental implications

Commonly, electron transfer is not initiated by an independent factor within a multicomponent system. Instead, it is more likely to be instigated by multiple factors in a synergistic manner (Chen et al., 2019a, b; Yu et al., 2020). In these processes, microbes might adjust their metabolisms, physiologies and other biotic interactions to optimize EET performance (Barberan et al., 2012). Notably, most *c*-cyts serve as critical carriers for delivering electrons in the EET process (Wang et al., 2019), making the electrical interplay between *c*-cyts and minerals a rapidly growing research topic (Shi et al., 2016). Previous investigations demonstrated that magnetite amendment could decrease the production of *c*-cyts in various microbial systems (Jin et al., 2019; Wang et al., 2018). However, many manganese oxides display similar physiochemical property with that of iron oxides, and their effects on production of *c*-cyts remains limited. Notably, our findings revealed a novel mechanism whereby MnO_2 stimulated microbe physiological behaviors by increasing the production of *c*-cyts. In contrast with traditional independent photocatalysis/microbial EET processes, MnO_2-assisted intimate coupling processes produced a greater amount of electrons and largely circumvented the inefficiency associated with independent processes to realize enhanced reaction efficacy. Considering manganese oxide minerals are abundant in natural environments, the biogeochemical cycling of As/Fe associated with pyrolusite (MnO_2) in soil is worthy of further consideration.

A schematic representation of the integrated mechanisms involved in regulation of As and Fe mobility in anoxic, arsenic-enriched soils by MnO_2 particles is shown in Fig. 8. Excited mineral photoelectron-hole pairs are separated in solar-irradiated soils due to scavenging of holes by soil humic/fulvic compounds, thereby enabling efficient photoelectron participation in microbial extracellular respiration processes. Additionally, an increased electron flux in illuminated flooded soils might also be supplied from the photodegradation of labile soil DOM by exogenous MnO_2 and/or other endogenous semiconducting minerals (Chen and Jaffe, 2016). These reactions supplied additional electrons to facilitate Fe(III)/As(V) reduction. Furthermore, MnO_2 amendment increased the abundance of metal-reducing bacteria (e.g., *Anaeromyxobacter*, *Bacillus*, *Geobacter,* and etc.), as well as increased production of *c*-cyts responsible for direct electron transfer. Additional factors, such as increased bioavailability of DOM as a substrate for metal-reducing bacteria and direct contact based EET processes via microbial nanowires, enhanced the reductive dissolution of Fe(III)/As(V) in flooded soils. Thereafter, a portion of the As(III) and Fe(II) released from the soil was attenuated by coupled adsorption/oxidation on MnO_2 surfaces. Precipitation of Fe/Mn hydr(oxides) on the MnO_2 surfaces provided additional reactive sites that enhanced further adsorption/oxidation of As(III)/Fe(II) in conjunction with complexation/coprecipitation of released Mn(II), that in turn reacted to produce As(V) and Fe(III).

Our findings enhanced the current understanding of the biogeochemical behaviors of As/Fe within a ternary "microbe-MnO_2-sunlight" composite system that is naturally occurring in flooded soils. This work demonstrated the efficacy of exploiting coupled microbial EET-photoelectrochemical technologies augmented with MnO_2 particles to enhance As migration from arsenic-polluted soils as a soil remediation strategy. Considering the economic and commercial accessibility of

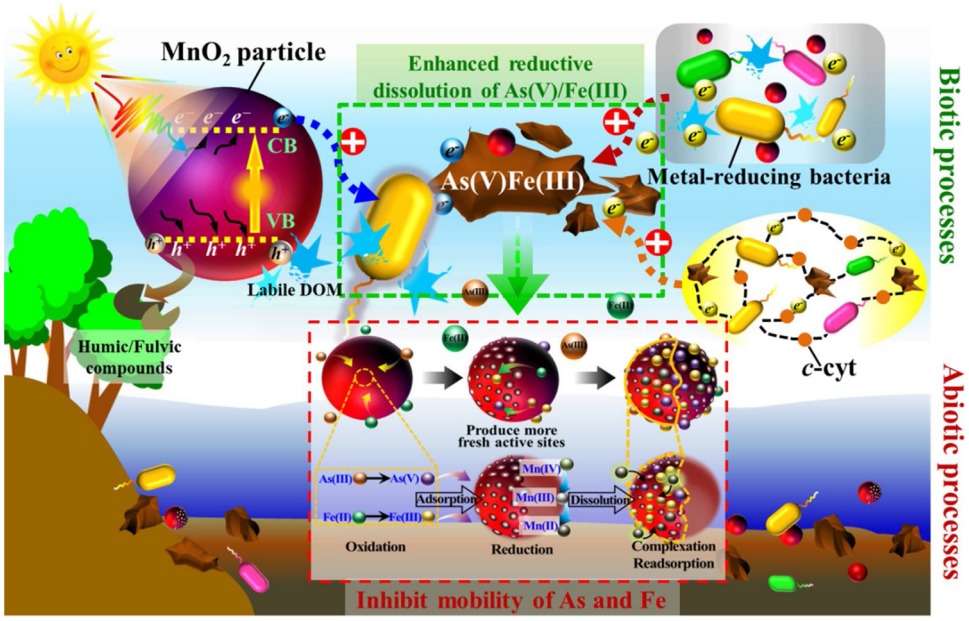

Fig. 8. Underlying mechanisms for migration pathways of Fe and As from flooded illuminated arsenic-enriched soils with MnO_2 amendment. Note: green and red dashed borders indicate abiotic and biotic processes, respectively.

MnO_2 particles, development of MnO_2-based regenerable adsorbents for As removal from wastewater have been deployed in recent years (Chen et al., 2018a; Ociński et al., 2016; Zhang et al., 2018). To maximize As removal, incorporating a MnO_2-based hybrid microbial-photoelectrochemical system confers several attractive advantages for remediation of arsenic-polluted soils. These coupled processes overcome several of the current inefficiencies associated with sequential processing and may be beneficial to realize rapid, continuous and efficient removal of As from arsenic-polluted soils in the future.

4. Conclusions

This study documented enhanced reductive dissolution of Fe(III)/As(V) from flooded soils under the combined treatment of MnO_2 amendment and intermittent illumination. Owing to the visible light-driven photocatalysis capability of MnO_2 particles, photoelectrons were generated upon illumination of the MnO_2-amended soils and fed into the microbial EET process, thus contributing more electrons for enhanced Fe(III)/As(V) reduction. The enhanced reductive-dissolution was also attributed to increased abundance of selected metal-reducing bacteria and production of *c*-cyts in the soil microbial community. Such regulation stimulated metal-reducing bacteria to degrade labile organic substrates to accelerate Fe/As reduction and facilitated more direct contact based EET processes. The cumulative impacts of MnO_2 particles on Fe/As reduction displayed a dose-response effect with higher concentrations resulting in greater Fe/As reduction. The mobility of a portion of the released Fe(II) and As(III) was attenuated due to a series of reactions with the MnO_2 particles that included adsorption, oxidation, complexation and/or coprecipitation. Overall, this study improved our mechanistic understanding of the functions of MnO_2 particles in regulating the biogeochemical fate and transport of As/Fe. These new findings demonstrated potential application for optimization of hybrid MnO_2 photocatalysis-microbial strategies for remediation of arsenic-polluted soils.

CRediT authorship contribution statement

Guowen Dong: Formal analysis, Investigation, Writing - original draft. **Ruiwen Han:** Conceptualization, Methodology, Software. **Yajing Pan:** Methodology, Software. **Chengkai Zhang:** Methodology, Software. **Yu Liu:** Methodology, Software. **Honghui Wang:** Investigation. **Xiaoliang Ji:** Investigation. **Randy A. Dahlgren:** Writing - review & editing. **Xu Shang:** Supervision. **Zheng Chen:** Writing - review & editing, Funding acquisition, Supervision. **Minghua Zhang:** Funding acquisition, Supervision.

Declaration of Competing Interest

The authors declare that they have no known competing financial interests or personal relationships that could have appeared to influence the work reported in this paper.

Acknowledgments

This work was supported by the National Natural Science Foundation of China (41807035 and 51979197), the Science and Technology Bureau of Wenzhou, China (G20190026) and the Research and Development Fund of Wenzhou Medical University (QTJ18034).

Appendix A. Supplementary data

Supplementary material related to this article can be found, in the online version, at doi:https://doi.org/10.1016/j.jhazmat.2020.123362.

References

Aklujkar, M., Coppi, M.V., Leang, C., Kim, B.C., Chavan, M.A., Perpetua, L.A., et al., 2013. Proteins involved in electron transfer to Fe(III) and Mn(IV) oxides by *Geobacter sulfurreducens* and *Geobacter uraniireducens*. Microbiol-Sgm 159, 515–535.
Barberan, A., Bates, S.T., Casamayor, E.O., Fierer, N., 2012. Using network analysis to explore co-occurrence patterns in soil microbial communities. ISME J. 6, 343–351.
Biesinger, M.C., Lau, L.W.M., Gerson, A.R., Smart, R.S.C., 2010. Resolving surface chemical states in XPS analysis of first row transition metals, oxides and hydroxides: Sc, Ti, V, Cu and Zn. Appl. Surf. Sci. 257, 887–898.
Chen, M.L., Jaffe, R., 2016. Quantitative assessment of photo- and bio-reactivity of chromophoric and fluorescent dissolved organic matter from biomass and soil leachates and from surface waters in a subtropical wetland. Biogeochemistry 129, 273–289.
Chen, X., Mao, S.S., 2007. Titanium dioxide nanomaterials: synthesis, properties, modifications, and applications. Chem. Rev. 107, 2891–2959.
Chen, Z., Wang, Y., Xia, D., Jiang, X., Fu, D., Shen, L., et al., 2016. Enhanced bioreduction of iron and arsenic in sediment by biochar amendment influencing microbial community composition and dissolved organic matter content and composition. J.

Hazard. Mater. 311, 20–29.
Chen, Z., Wang, Y., Jiang, X., Fu, D., Xia, D., Wang, H., et al., 2017. Dual roles of AQDS as electron shuttles for microbes and dissolved organic matter involved in arsenic and iron mobilization in the arsenic-rich sediment. Sci. Total Environ. 574, 1684–1694.
Chen, J., Wang, J., Zhang, G., Wu, Q., Wang, D., 2018a. Facile fabrication of nanostructured cerium-manganese binary oxide for enhanced arsenite removal from water. Chem. Eng. J. 334, 1518–1526.
Chen, Z., Dong, G., Gong, L., Li, Q., Wang, Y., 2018b. The role of low-molecular-weight organic carbons in facilitating the mobilization and biotransformation of As(V)/Fe (III) from a realgar tailing mine soil. Geomicrobiol. J. 35, 555–563.
Chen, Z., Li, H., Ma, W., Fu, D., Han, K., Wang, H., et al., 2018c. Addition of graphene sheets enhances reductive dissolution of arsenic and iron from arsenic contaminated soil. Land. Degrad. Dev. 29, 572–584.
Chen, Z., Dong, G., Chen, Y., Wang, H., Liu, S., Chen, Z., et al., 2019a. Impacts of enhanced microbial-photoreductive and suppressed dark microbial reductive dissolution on the mobility of As and Fe in flooded tailing soils with zinc sulfide. Chem. Eng. J. 372, 118–128.
Chen, Z., Liu, Y., Zhang, C., Pan, Y., Han, R., Chen, Y., et al., 2019b. Titanium dioxide nanoparticles induced an enhanced and intimately coupled photoelectrochemical-microbial reductive dissolution of As(V) and Fe(III) in flooded arsenic-enriched soils. ACS Sustain. Chem. Eng. 7, 13236–13246.
Chen, Z., Zhang, Y., Luo, Q., Wang, L., Liu, S., Peng, Y., et al., 2019c. Maghemite (γ-Fe_2O_3) nanoparticles enhance dissimilatory ferrihydrite reduction by *Geobacter sulfurreducens*: impacts on iron mineralogical change and bacterial interactions. J. Environ. Sci. 78, 193–203.
Chhabra, T., Kumar, A., Bahuguna, A., Krishnan, V., 2019. Reduced graphene oxide supported MnO_2 nanorods as recyclable and efficient adsorptive photocatalysts for pollutants removal. Vacuum 160, 333–346.
Cockayne, E., Li, L., 2012. First-principles DFT + U studies of the atomic, electronic, and magnetic structure of α-MnO_2 (cryptomelane). Chem. Phys. Lett. 544, 53–58.
Crimi, M., Ko, S., 2009. Control of manganese dioxide particles resulting from in situ chemical oxidation using permanganate. Chemosphere 74, 847–853.
Darmane, Y., Cherkaoui, M., Kitane, S., Alaoui, A., Sebban, A., Touhami, M.E., 2008. Preparation of chemical manganese dioxide from Moroccan pyrolusite mine waste. Hydrometallurgy 92, 73–78.
Farías, S.S., Londonio, A., Quintero, C., Befani, R., Soro, M., Smichowski, P., 2015. Online speciation and quantification of four arsenical species in rice samples collected in Argentina using a HPLC–HG–AFS coupling. Microchem. J. 120, 34–39.
Gorby, Y.A., Yanina, S., McLean, J.S., Rosso, K.M., Moyles, D., Dohnalkova, A., et al., 2006. Electrically conductive bacterial nanowires produced by *Shewanella oneidensis* strain MR-1 and other microorganisms. Proc. Natl. Acad. Sci. U. S. A. 103, 11358–11363.
Gorny, J., Billon, G., Lesven, L., Dumoulin, D., Made, B., Noiriel, C., 2015. Arsenic behavior in river sediments under redox gradient: a review. Sci. Total Environ. 505C, 423–434.
Han, L., Sun, K., Jin, J., Xing, B., 2016. Some concepts of soil organic carbon characteristics and mineral interaction from a review of literature. Soil Biol. Biochem. 94, 107–121.
Hernandez, M.E., Newman, D.K., 2001. Extracellular electron transfer. Cell. Mol. Life Sci. 58, 1562–1571.
Jin, Z., Zhao, Z., Zhang, Y., 2019. Potential of direct interspecies electron transfer in synergetic enhancement of methanogenesis and sulfate removal in an up-flow anaerobic sludge blanket reactor with magnetite. Sci. Total Environ. 677, 299–306.
Kitchaev, D.A., Dacek, S.T., Sun, W., Ceder, G., 2017. Thermodynamics of phase selection in MnO_2 framework structures through alkali intercalation and hydration. J. Am. Chem. Soc. 139, 2672–2681.
Koo, M.S., Cho, K., Yoon, J., Choi, W., 2017. Photoelectrochemical degradation of organic compounds coupled with molecular hydrogen generation using electrochromic TiO_2 nanotube arrays. Environ. Sci. Technol. 51, 6590–6598.
Kumar, A., Aathira, M.S., Pal, U., Jain, S.L., 2018. Photochemical oxidative coupling of 2-naphthols using a hybrid reduced graphene oxide/manganese dioxide nanocomposite under visible-light irradiation. ChemCatChem 10, 1844–1852.
Lenoble, V., Laclautre, C., Serpaud, B., Deluchat, V., Bollinger, J.-C., 2004. As(V) retention and As(III) simultaneous oxidation and removal on a MnO_2-loaded polystyrene resin. Sci. Total Environ. 326, 197–207.
Li, Q.Q., Xie, L., Jiang, Y., Fortner, J.D., Yu, K., Liao, P., et al., 2019a. Formation and stability of NOM-Mn(III) colloids in aquatic environments. Water Res. 149, 190–201.
Li, Y., Luo, Q., Li, H., Chen, Z., Shen, L., Peng, Y., et al., 2019b. Application of 2-hydroxy-1, 4-naphthoquinone-graphene oxide (HNQ-GO) composite as recyclable catalyst to enhance Cr(VI) reduction by *Shewanella xiamenensis*. J. Chem. Technol. Biotechnol. 94, 446–454.
Liu, C., Luo, C., Gao, Y., Li, F., Lin, L., Wu, C., et al., 2010. Arsenic contamination and potential health risk implications at an abandoned tungsten mine, southern China. Environ. Pollut. 158, 820–826.
Liu, F., Rotaru, A.-E., Shrestha, P.M., Malvankar, N.S., Nevin, K.P., Lovley, D.R., 2015. Magnetite compensates for the lack of a pilin-associated c-type cytochrome in extracellular electron exchange. Environ. Microbiol. 17, 648–655.
Liu, X., Shi, L., Gu, J.-D., 2018. Microbial electrocatalysis: redox mediators responsible for extracellular electron transfer. Biotechnol. Adv. 36, 1815–1827.
Lu, A.H., Li, Y., Jin, S., Wang, X., Wu, X.L., Zeng, C.P., et al., 2012. Growth of non-phototrophic microorganisms using solar energy through mineral photocatalysis. Nat. Commun. 3, 1–8.
Lu, A.H., Wang, X., Li, Y., Ding, H.R., Wang, C.Q., Zeng, C.P., et al., 2014. Mineral photoelectrons and their implications for the origin and early evolution of life on Earth. Sci. China. Earth. Sci. 57, 897–902.
Lu, A., Li, Y., Ding, H., Xu, X., Li, Y., Ren, G., et al., 2019. Photoelectric conversion on Earth's surface via widespread Fe- and Mn-mineral coatings. Proc. Natl. Acad. Sci. U. S. A. 116, 9741–9746.
Ma, L., Cai, D., Tu, S., 2020. Arsenite simultaneous sorption and oxidation by natural ferruginous manganese ores with various ratios of Mn/Fe. Chem. Eng. J. 382, 123040.
Nishimura, T., Umetsu, Y., 2001. Oxidative precipitation of arsenic(III) with manganese (II) and iron(II) in dilute acidic solution by ozone. Hydrometallurgy 62, 83–92.
Ociński, D., Jacukowicz-Sobala, I., Mazur, P., Raczyk, J., Kociołek-Balawejder, E., 2016. Water treatment residuals containing iron and manganese oxides for arsenic removal from water – characterization of physicochemical properties and adsorption studies. Chem. Eng. J. 294, 210–221.
Qiao, J.T., Li, X.M., Hu, M., Li, F.B., Young, L.Y., Sun, W.M., et al., 2018a. Transcriptional activity of arsenic-reducing bacteria and genes regulated by lactate and biochar during arsenic transformation in flooded paddy soil. Environ. Sci. Technol. 52, 61–70.
Qiao, J.T., Li, X.M., Li, F.B., 2018b. Roles of different active metal-reducing bacteria in arsenic release from arsenic-contaminated paddy soil amended with biochar. J. Hazard. Mater. 344, 958–967.
Qiao, J., Li, X., Li, F., Liu, T., Young, L.Y., Huang, W., et al., 2019. Humic substances facilitate arsenic reduction and release in flooded paddy soil. Environ. Sci. Technol. 53, 5034–5042.
Reguera, G., McCarthy, K.D., Mehta, T., Nicoll, J.S., Tuominen, M.T., Lovley, D.R., 2005. Extracellular electron transfer via microbial nanowires. Nature 435, 1098–1101.
Richardson, D.J., Butt, J.N., Fredrickson, J.K., Zachara, J.M., Shi, L., Edwards, M.J., et al., 2012. The' porin-cytochrome' model for microbe-to-mineral electron transfer. Mol. Microbiol. 85, 201–212.
Sachdev, S.L., Robinson, J.W., West, P.W., 1967. Determination of manganese, iron, cobalt and nickel in air and water by atomic absorption spectroscopy. Anal. Chim. Acta 38, 499–506.
Shi, L., Dong, H., Reguera, G., Beyenal, H., Lu, A., Liu, J., et al., 2016. Extracellular electron transfer mechanisms between microorganisms and minerals. Nat. Rev. Microbiol. 14, 651–662.
Thanh, D.N., Singh, M., Ulbrich, P., Štěpánek, F., Strnadová, N., 2012. As(V) removal from aqueous media using α-MnO_2 nanorods-impregnated laterite composite adsorbents. Mater. Res. Bull. 47, 42–50.
Wang, D., Han, Y., Han, H., Li, K., Xu, C., Zhuang, H., 2018. New insights into enhanced anaerobic degradation of Fischer-Tropsch wastewater with the assistance of magnetite. Bioresour. Technol. Rep. 257, 147–156.
Wang, F., Gu, Y., O'Brien, J.P., Yi, S.M., Yalcin, S.E., Srikanth, V., et al., 2019. Structure of microbial nanowires reveals stacked hemes that transport electrons over micrometers. Cell 177, 361-369.e10.
Xiong, Y., Tong, Q., Shan, W., Xing, Z., Wang, Y., Wen, S., et al., 2017. Arsenic transformation and adsorption by iron hydroxide/manganese dioxide doped straw activated carbon. Appl. Surf. Sci. 416, 618–627.
Xu, Y., Schoonen, M.A.A., 2000. The absolute energy positions of conduction and valence bands of selected semiconducting minerals. Am. Mineral. 85, 543–556.
Xu, H., Yu, G., Yang, L., Jiang, H., 2013. Combination of two-dimensional correlation spectroscopy and parallel factor analysis to characterize the binding of heavy metals with DOM in lake sediments. J. Hazard. Mater. 263, 412–421.
Xue, S., Shi, L., Wu, C., Wu, H., Qin, Y., Pan, W., et al., 2017. Cadmium, lead, and arsenic contamination in paddy soils of a mining area and their exposure effects on human HEPG2 and keratinocyte cell-lines. Environ. Res. 156, 23–30.
Yang, X., Li, Y., Lu, A., Yan, Y., Wang, C., Wong, P.-K., 2011. Photocatalytic reduction of carbon tetrachloride by natural sphalerite under visible light irradiation. Sol. Energy Mater. Sol. Cells 95, 1915–1921.
Yu, M., Wang, J., Tang, L., Feng, C., Liu, H., Zhang, H., et al., 2020. Intimate coupling of photocatalysis and biodegradation for wastewater treatment: mechanisms, recent advances and environmental applications. Water Res. 175, 115673.
Zhang, W., Liu, C., Zheng, T., Ma, J., Zhang, G., Ren, G., et al., 2018. Efficient oxidation and sorption of arsenite using a novel titanium(IV)-manganese(IV) binary oxide sorbent. J. Hazard. Mater. 353, 410–420.